PHYSICAL REVIEW B VOLUME 27, NUMBER 4 15 FEBRUARY 1983

Further characterization of the E_1' center in crystalline SiO_2

M. G. Jani, R. B. Bossoli, and L. E. Halliburton
Physics Department, Oklahoma State University, Stillwater, Oklahoma 74078
(Received 21 October 1982)

Electron-spin resonance (ESR) is used to investigate the formation and thermal anneal characteristics of E_1' centers in high-quality synthetic quartz. These centers are produced by ionizing radiation near room temperature followed by annealing to 300 °C. The resulting concentration depends on the specific irradiation temperature, the nature of previous irradiation and thermal anneals, and whether the sample is air swept or unswept. Migration of interstitial alkali ions (Li^+ and/or Na^+) as a result of irradiation correlates with the production of the E_1' centers, and a relationship between the $[AlO_4]^0$-center concentration and the E_1'-center concentration is also observed. Electron-nuclear double resonance is used to show that the two "weak" hyperfine interactions (8- and 9-G splittings) are with ^{29}Si nuclei. From the angular dependence of the ESR data taken at 300 K, complete sets of spin-Hamiltonian parameters are determined for the $\tilde{g}$ matrix and the three ^{29}Si hyperfine (one strong and two weak) matrices.

I. INTRODUCTION

The E_1' center is a fundamental point defect in α-quartz. Using electron spin resonance (ESR), Weeks[1] was the first to observe this center, and the angular dependence of its ESR spectrum was later characterized in detail by Silsbee.[2] In the mid 1970s, theoretical investigations of the E_1' center were undertaken by Feigl *et al.*[3] and Yip and Fowler,[4] and comparisons were made with the spin-Hamiltonian parameters obtained by Silsbee. Their calculations resulted in the presently accepted model of the E_1' center; namely, an oxygen vacancy having an unpaired electron localized in the sp^3 hybrid orbital extending into the vacancy from the adjacent silicon ion on the short-bond side of the vacancy.

Numerous additional studies[5–13] of defects in α-quartz and silica glass have focused on the E_1' center during the past 25 years. However, despite the wide attention given to this defect, significant questions remain about the formation and stabilization mechanisms and about its electronic and ionic structure. For example, the criteria for production of this center are not fully established: Weeks[1] and Silsbee[2] both used fast-neutron irradiation, with attendant heating of the sample, to produce the E_1' centers; whereas more recent studies[5,7,9] have reported that a room-temperature irradiation with only ionizing radiation (e.g., x rays) followed by a thermal anneal to approximately 300 °C produces E_1' centers. When the E_1' centers are created in this latter way by ionizing radiation, the identity of the centers' precursor becomes of interest; but no definitive results pertaining to this precursor have been reported. Equally perplexing has been the interpretation of the observed "weak" hyperfine spectrum (two doublets with 8- and 9-G c-axis splittings). It has been generally accepted that these doublets were due to ^{29}Si nuclei, but Griscom[13] has raised the possibility that they may be due to protons instead. Another area of uncertainty is possible motional effects for the E_1' center. The single—oxygen-vacancy model[3,4] of Feigl, Fowler, and Yip suggests that the unpaired electron and its associated asymmetric lattice relaxation should be found, at least for observable periods of time at certain temperatures, on the opposite side of the vacancy; but no supporting data for such effects have been reported yet. Thus it is quite apparent that gaps exist in our understanding of the E_1' center in α-quartz.

The purpose of the present paper is to provide a description of the production and thermal decay properties of the E_1' centers created by ionizing radiation and to further characterize the magnetic resonance spectra of the E_1' centers. This information will be useful in developing a more detailed model of the center and in identifying its precursor state. ESR and electron-nuclear double resonance (ENDOR) are the primary experimental tools used in this study, and both unswept and swept samples of commercially available, high-quality synthetic quartz are used. As part of our study, the concentrations of $[AlO_4]^0$ centers and E_1' centers, determined after different thermal anneals and irradiation treatments, have been compared in a variety of samples.

II. EXPERIMENTAL PROCEDURE

A right-handed crystal coordinate system (X, Y, and Z) is used in our work and the direction of the $+X$ axis (parallel to $+\vec{a}_1$) for each crystal was determined by a "squeeze" test, i.e., the positive end of the X axis develops a negative charge during compression.[14] Lumbered bars of pure z-growth right-handed synthetic quartz were obtained from Sawyer Research Products, Eastlake, Ohio, from Toyo Communications Equipment Company, Japan, and from Western Electric. Samples having typical dimensions of $7\times3\times2$ mm^3 in the X, Y, and Z directions, respectively, were cut from these bars for use in the ESR studies and were labeled according to the scheme introduced by Markes and Halliburton.[15]

A Van de Graaff accelerator (1.7-MeV electrons) was used for all irradiations and the incident electron current on the samples was 0.2 μA. Irradiation times were 10 min at room temperature and 4 min at 77 K and intermediate temperatures. The samples were immersed in liquid nitrogen for the irradiations at 77 K while nitrogen gas of the desired temperature flowed by the sample during the variable temperature irradiation sequence between 77 and 350 K. The ESR spectra for the $[AlO_4]^0$ centers were monitored at 77 K, while the ESR spectra for the E_1' centers were recorded at 300 K. All the thermal anneals were done using a small benchtop furnace. After the furnace had reached the desired temperature the sample was placed inside the furnace, and then removed after 15 min.

The homodyne ESR spectrometer utilized a home-built microwave bridge, operating at X band and containing a detector-bias arm. A Narda N6244S-37 microwave solid-state amplifier was added to the bridge to increase sensitivity, especially at lower microwave-power levels. A Varian V-4531 rectangular cavity was used and the static magnetic field was modulated at 100 kHz. Magnetic field positions were measured with a Varian E-500 digital self-tracking gaussmeter and the microwave frequencies were monitored with a Hewlett-Packard HP-5340A microwave counter. Corrections for magnetic field differences between the gaussmeter probe and the sample were made using a standard MgO:Cr^{3+} crystal ($g=1.9799$). All ESR data were taken with approximately 0.4 mW of microwave power incident on the cavity and with the spectrometer's phase detector set "out of phase."

The ESR spectrometer was modified for ENDOR operation by adding an HP-8601A sweep generator, rf power amplifier, and a Nicolet 1073 signal averager. The static field modulation at 100 kHz was retained. A three-turn rf coil was placed inside a large-sample Varian E-235 cavity, and the combination of coil and sample was cooled to 112 K by flowing nitrogen gas. Data were obtained by sweeping the rf across the frequency range of interest at a rate of approximately 5 sweeps/sec and accumulating any changes of the ESR signal intensity in the signal averager. Typically, 2000 sweeps would be needed to acquire adequate signal-to-noise ratios. The quartz sample used in the ENDOR study was from Western Electric and had dimensions of $13.9\times10.0\times2.7$ mm^3 in the X, Y, and Z directions, respectively.

III. RESULTS

A. Production and anneal behavior

The ESR spectrum of the E_1' centers in quartz is shown in Fig. 1 for the case when the magnetic field is parallel to the c axis of the crystal. A single intense line dominates the spectrum for this orientation and is surrounded by two pairs of weak hyperfine lines having splittings of 8.02 and 9.12 (hereafter referred to as 8- and 9-G splittings). Also observed is an additional pair of lines approximately centered on the main line and having a splitting of 403.6 G. These latter lines are due to a strong hyperfine interaction with one ^{29}Si nucleus.[12]

The production of the E_1' centers in quartz is strongly dependent on prior sample treatments. The E_1' centers are easily produced in an unswept sample by a 15-min anneal at 300 °C provided the sample has been previously irradiated at room temperature. A similar anneal after only irradiation at 77 K of an as-grown unswept sample forms a much smaller concentration of the E_1' centers.

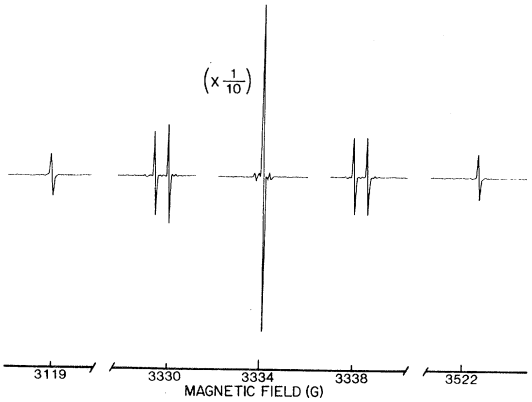

FIG. 1. Electron-spin-resonance spectrum of the E_1' center. Magnetic field is parallel to the c axis, microwave frequency is 9.3358 GHz, and temperature is 297 K. Spectrometer gain was reduced by a factor of 10 for the large center line and the entire spectrum was taken with a constant magnetic field sweep rate.

A thermal anneal study in the region above room temperature was done on two as-grown unswept Toyo samples, labeled 1 and 2. Both samples were irradiated at 300 K, and then further irradiated at 77 K. Sample no. 1 was annealed at 300 °C for 15 min after the 77-K irradiation in order to eliminate the $[AlO_4]^0$ centers and leave only E_1' centers. At this stage, both samples were subjected to a pulsed thermal-anneal sequence beginning at room temperature, and the results are shown in Fig. 2. After holding the samples at a specific temperature for 15 min, the concentrations of $[AlO_4]^0$ centers were monitored at 77 K and the concentrations of E_1' centers were monitored at room temperature. In sample no. 2 (represented by open circles in Fig. 2) the $[AlO_4]^0$ centers were observed to anneal out by 300 °C and the E_1' centers appeared above 200 °C and reached their maximum intensity at 300 °C. The E_1' centers thermally annealed near 425 °C for both samples nos. 1 and 2 (represented by filled circles in Fig. 2).

A variable-temperature irradiation study in the range 77–350 K was performed on an as-grown Toyo quartz sample. The results are plotted in Fig. 3. After each irradiation, the sample was returned to room temperature. The $[AlO_4]^0$ centers resulting from each irradiation step were monitored at 77 K. At each step, this was followed by an anneal at 300 °C for 15 min to produce the E_1' centers, and their concentration was monitored at room temperature. After each determination of the $[AlO_4]^0$ and the E_1'-center concentrations, the sample was irradiated at the next-higher temperature and the measurement sequence was repeated. As shown in Fig. 3, the 15-min anneal at 300 °C will not form the E_1' centers unless the sample has been previously irradiated above 200 K. An interesting feature of the data in Fig. 3 is that even though the $[AlO_4]^0$ center concentration reaches its maximum value (i.e., saturates) after the irradiation at 270 K, the E_1'-center concentration increases with further irradiations at higher temperatures.

Now that it has been shown that irradiations above 200 K are a necessary condition for the production of the E_1' centers, the anneal temperature required to restore an unswept sample to its as-grown state must be determined. The results shown in Fig. 4 were obtained in the following way. First, the sample was irradiated at room temperature, then it

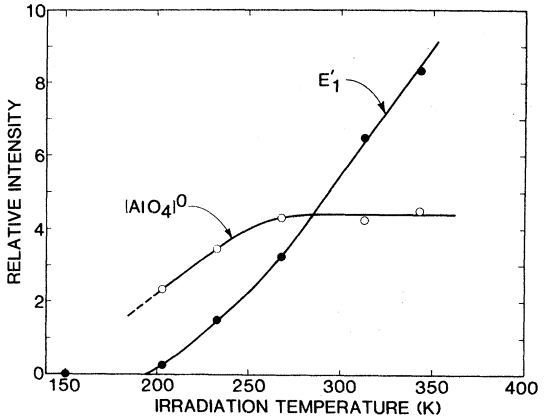

FIG. 3. Production of E_1' and $[AlO_4]^0$ centers by radiation at various temperatures. Sample was subjected to the following sequence after each irradiation: (1) taken to room temperature, (2) cooled to 77 K where the $[AlO_4]^0$ centers were monitored, (3) annealed to 300 °C, and (4) returned to room temperature where the E_1' centers were monitored.

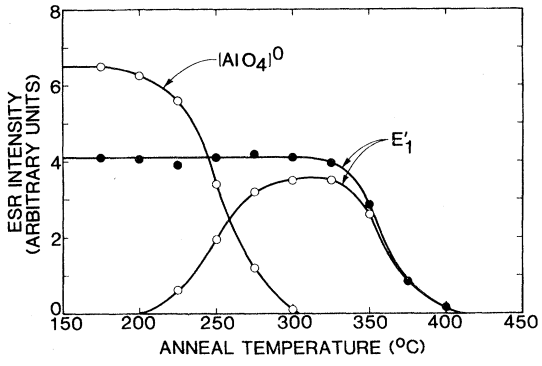

FIG. 2. Thermal anneal of the E_1' and $[AlO_4]^0$ centers. Following each 15-min anneal step, the E_1' centers and $[AlO_4]^0$ centers were monitored at room temperature and 77 K, respectively. Both samples were initially irradiated at 300 and then at 77 K, and the sample represented by the filled circles was then heated to 300 °C before beginning the anneal sequence.

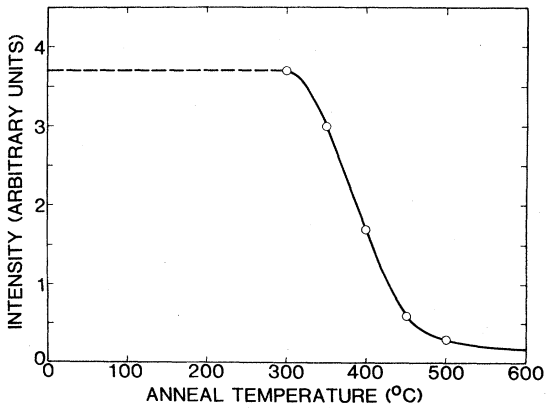

FIG. 4. Effect of high-temperature annealing on the production of E_1' centers by the combination of room-temperature irradiation and 300 °C anneal.

was irradiated at 77 K, next it was annealed to 300 °C for 15 min, and finally the E_1'-center concentration was measured at room temperature. This gave the data point plotted at 300 °C in Fig. 4. For the remaining data, the sample was annealed to the particular temperature above 300 °C and then irradiated at 77 K, after which the sample was annealed to 300 °C for 15 min and the resulting E_1'-center concentration was monitored at room temperature. As shown in Fig. 4, an anneal above 450 °C returns the quartz sample to its as-grown state (i.e., the sample is recycled).

Various swept and unswept samples were studied to establish a possible correlation between the concentrations of the $[AlO_4]^0$ centers and the E_1' centers. Each sample was irradiated for 8 min at 300 K and then immediately irradiated for 4 min at 77 K. Following the irradiation at 77 K, the $[AlO_4]^0$ center concentration was monitored before and after warming the sample to room temperature. The $[AlO_4]^0$-center concentration initially measured at 77 K represents the total aluminum content (in arbitrary units) for each sample.[15] The sample was then thermally annealed at 200 °C for 15 min and the $[AlO_4]^0$ centers were monitored following this anneal. Finally, the sample was thermally annealed at 300 °C for 15 min and the resulting E_1' centers were monitored at room temperature. Results of this study are presented in Table I. The ratio of the $[AlO_4]^0$ centers at 200 °C to the E_1' centers remains nearly constant, ranging from 0.875 to 1.35 for the various samples despite a considerably larger variation in aluminum content.

B. Magnetic resonance spectra

Spin-Hamiltonian parameters for the E_1' center have been previously reported by Silsbee.[2] However, due to the existing confusion in the quartz ESR literature concerning conventions for specifying principal-axes directions, we felt it useful to redetermine the various spin-Hamiltonian matrices for the E_1' center. Also, since the identities of the two nuclei giving rise to the weak hyperfine interactions (8- and 9-G c-axis splittings) have been questioned,[13] an ENDOR experiment was initiated.

Results of our ENDOR investigation are summarized in Fig. 5. They clearly show that ^{29}Si is the nucleus responsible for both the 8- and 9-G c-axis splittings. At 112 K where the ENDOR data were obtained, these splittings were actually 8.30 and 9.09 G, respectively. The ENDOR spectrum in Fig. 5(a) was obtained from the high-field ESR line of the 9-G hyperfine pair. It contains two ENDOR transitions, one at 10.008 MHz and the other at 15.417 MHz. The ENDOR spectrum in Fig. 5(b) came

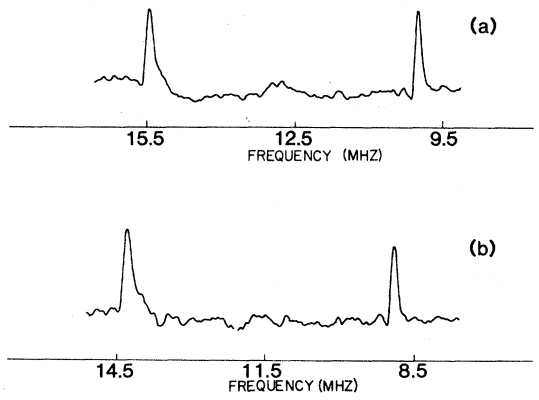

FIG. 5. Electron-nuclear double-resonance spectra obtained from the weak hyperfine interactions of the E_1' centers. Sample temperature was 112 K, microwave frequency was 9.0644 GHz, and magnetic field was parallel to the c axis. Trace (a) was taken on the high-field line (3239.3 G) of the 9-G hyperfine pair, and trace (b) was taken on the high-field line (3238.9 G) of the 8-G hyperfine pair.

from the high-field ESR line of the 8-G hyperfine pair and it contains ENDOR transitions at 8.887 and 14.323 MHz. To first order, the separation between each set of ENDOR lines should be $2\nu_N$ and the average of the two ENDOR lines should be $A/2$, provided $\nu_N < A/2$. For a ^{29}Si nucleus, the nuclear resonance frequency ν_N is 2.740 MHz for a 3239.1-G magnetic field, and we see that twice this ν_N value is very close to our experimentally observed separations.

The ESR spectrum of the E_1' center is shown in Fig. 1 for the magnetic field parallel to the c axis. When the magnetic field is changed to an arbitrary direction, every line in the c-axis ESR spectrum splits into six lines due to the six inequivalent oxygen sites in the crystal. Since the X axis of the crystal is a twofold axis, the ESR spectrum at various orientations within the X plane consists of only three lines corresponding to each initial line in the c-axis spectrum. An angular dependence study for the main line and the three ^{29}Si hyperfine doublets, one strong and two weak, was done at 300 K with the magnetic field always in the plane perpendicular to the X axis of the crystal.

The spin-Hamiltonian matrices $\overleftrightarrow{g}$, $\overleftrightarrow{A}_{\text{strong}}$, $\overleftrightarrow{A}_{1,\text{weak}}$, and $\overleftrightarrow{A}_{2,\text{weak}}$ were calculated using the following spin-Hamiltonian:

$$\mathcal{H}=\mu\vec{S}\cdot\overleftrightarrow{g}\cdot\vec{H}+\vec{S}\cdot\overleftrightarrow{A}\cdot\vec{I}-g_N\mu_N\vec{H}\cdot\vec{I}\ .$$

The first term represents the electron Zeeman interaction, the second term represents the hyperfine interaction, and the last term accounts for the nuclear Zeeman interaction.

Final parameter values were obtained by using a least-squares-fit computer program to repeatedly diagonalize[16] the 4×4 Hamiltonian matrix. Measured microwave frequencies and magnetic field values were provided as input data to this program. These best sets of parameter values are listed in Table II along with the total number of angles and line positions used in each of the fittings and the resulting root-mean-square deviations. We assume that the ^{29}Si hyperfine values are all negative, in accordance with the sign of the nuclear magnetic moment. Specification of principal axes directions in Table II is by means of (θ,ϕ) angles, where θ is measured relative to the $+Z$ direction and ϕ is measured relative to the $+X$ direction in the Z plane with positive rotation being the $+X$ to the $+Y$ direction. The $\tilde{g}$ matrix parameters presented in Table II were obtained from the angular dependence of those E_1' centers having no resolved hyperfine, i.e., no ^{29}Si near neighbors. The g values were also recalculated during each of the hyperfine matrix fittings and agreement between the four sets of g values was excellent (principal values and unique axis angles varied by less than 0.000 015 and 0.6°, respectively). Finally, the angular dependence curves calculated from the final parameters are shown in Figs. 6 and 7.

IV. DISCUSSION

From the data presented in this paper, it is evident that interstitial alkali-metal ions have an influence on the production and/or stabilization of E_1' centers in α-quartz. Whether this influence is of a direct or indirect nature has not been clearly determined, but the results do indicate certain relationships between the presence and behavior of interstitial alkali-metal ions and the formation of E_1' centers. Also, it is obvious from our data that additional factors, besides the interstitiitial alkali-metal ion question, are involved in the production of E_1' centers.

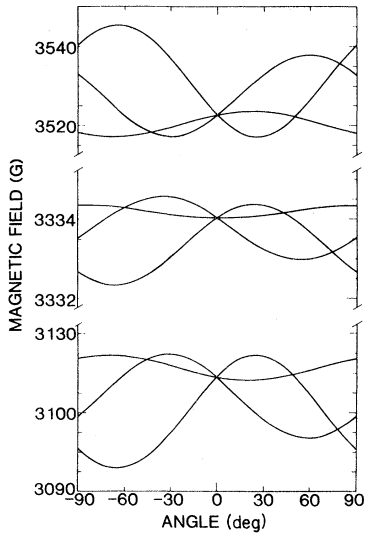

FIG. 6. Angular dependence of the central large lines (i.e., lines due to centers without ^{29}Si near neighbors) and the strong ^{29}Si hyperfine for the E_1' centers in α-quartz. Rotation of the magnetic field is in the plane perpendicular to the X axis of the crystal.

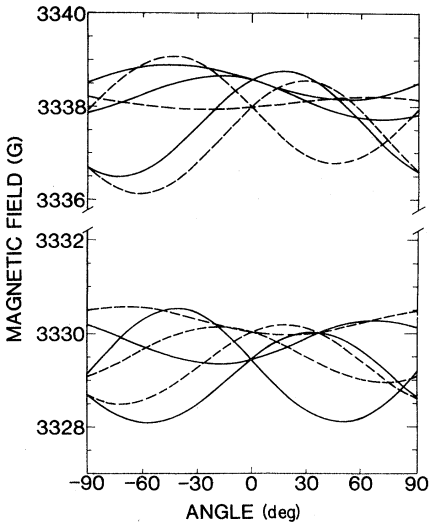

FIG. 7. Angular dependence of the two weak ^{29}Si hyperfine interactions for the E_1' centers in α-quartz. Rotation of the magnetic field is in the plane perpendicular to the X axis of the crystal.

In the past, studies of the radiation-induced mobility of interstitial alkali-metal ions have led to an enhanced understanding of point defects in α-quartz. These interstitial alkali-metal ions are present as charge compensators in all as-grown quartz and they are initially localized next to the substitutional Al^{3+} ions. It has been shown by Markes and Halliburton[15] that the interstitial alkali-metal ions become mobile under irradiation at temperatures above 200 K. This observation is additionally supported by the acoustic loss measurements of Doherty *et al.*[17] Upon release by radiation, the interstitial alkali-metal ions diffuse along the c-axis channels and become stably trapped at unknown sites within the crystal. Annealing the sample above 750 K allows these interstitial alkali-metal ions to return from their unknown trapping sites to the Al^{3+} sites, and thereby restores the crystal to its as-grown configuration.

A major feature of the present study is that the E_1' centers produced as a result of ionizing radiation can be found in large concentration only in unswept or in partially swept quartz (i.e., the E_1' centers can

be easily formed only when interstitial alkali ions are present in the crystal). However, there is no evidence of direct association of the interstitial alkali-metal ions with the E_1' center, a result in agreement with previous studies. Also, we have observed that the E_1' centers cannot be formed unless the sample has been irradiated above 200 K, which is the necessary condition for mobility of interstitial alkali-metal ions away from the Al^{3+} sites. It is interesting to note that similar production behavior has been found for the E'' centers (i.e., pairs of oxygen vacancies) in quartz.[18]

Our study has verified that room-temperature irradiation by itself does not readily form E_1' centers, whereas a 15-min thermal anneal at 300 °C following a room-temperature irradiation enhances the E_1' center concentration at least by a factor of 20. These results suggest that the formation of the E_1' center is a two-step process. The initial room-temperature irradiation changes "precursor" defects present in an as-grown crystal into an intermediate state which is then converted into E_1' centers by the subsequent 15-min thermal anneal at 300 °C.

In order to fully understand the E_1' centers, their precursors must be identified. Based on the limited data available from past studies, it has been generally assumed that the precursor of the E_1' center is an oxygen vacancy containing two electrons in a singlet state ($S=0$). The results in Table I do not disagree with this possibility. From Table I, we see that the ratio of $[AlO_4]^0$ centers, present after the 200 °C anneal, to the E_1' centers, produced by the 300 °C anneal, is nearly constant. Thus, when combined with the data in Fig. 2, one could imagine that holes are released from the $[AlO_4]^0$ centers during their anneal in the 200–300 °C range, and that each of these holes recombines with one of the electrons in each vacancy to form the E_1' centers. However, the production data shown in Fig. 3, where the E_1'-center concentration continues to grow after the $[AlO_4]^0$-center concentration has saturated, do not appear to agree with this simple formation mechanism for the E_1' centers. The production and thermal-anneal characteristics presented in this paper suggest that the precursors of the E_1' centers are more complex.

The ENDOR study of the E_1' center has shown that the two weak hyperfine interactions are with ^{29}Si nuclei, and the ESR angular dependence study has allowed us to obtain a best set of parameter values for the spin-Hamiltonian matrices. Those values presented in Table II correspond to one particular site in the crystal, out of six possible sites, and the angles for the other five sets will be $(\theta,\phi\pm120°)$, $(180°-\theta,-\phi)$, and $(180°-\theta,-\phi\pm120°)$. The principal values previously obtained by Silsbee[2] are presented in Table II along with our present results and, as can be seen, there is excellent agreement between the two sets of data. We do not make a comparison between our principal-axes directions and those determined by Silsbee because of a lack of knowledge about the coordinate system and $+X$-axis choice used by Silsbee.

ESR data have proven to be the most useful in developing the model for the E_1' center. The $\overleftrightarrow{g}$ matrix and the hyperfine matrices are nearly axial and the direction of their unique axes can be compared to the various bond directions[19] in the perfect quartz lattice. The normal-lattice bond lengths and bond directions are given in Table III along with the position coordinates for the atoms. The notation used in Table III for the silicon and oxygen atoms is based upon Fig. 8. In this figure O(1) and O(2) form the short bonds relative to Si(0) and O(3) and O(4) form the long bonds relative to Si(0). The unique axes of the $\overleftrightarrow{g}$ matrix and strong hyperfine matrix are nearly collinear and agree excellently with the Si(0)–O(1) bond direction. This led Feigl *et al.*[3] and Yip and Fowler[4] to propose an asymmetrical relaxation of

TABLE I. Relative concentrations of $[AlO_4]^0$ centers and E_1' centers at various anneal stages following an irradiation at 300 K and then at 77 K. Samples 7 and 8 had been previbeen previously swept in air; the other samples were unswept. The arbitrary units for the $[AlO_4]^0$ concentrations are not necessarily equivalent to the arbitrary units for the E_1' concentrations.

Sample	$[AlO_4]^0$ at 77 K	$[AlO_4]^0$ at room temperature	$[AlO_4]^0$ after 200 °C anneal	E_1' after 300 °C anneal	Ratio of $[AlO_4]^0$ after 200 °C anneal to E_1'
3	92	34	25	21	1.19
4	17	7.1	5.2	5.6	0.93
5	120	81	63	46.5	1.35
6	71	43	43	49	0.88
7	43	16.2	8.4	7.1	1.18
8	24	4.3	2.1	2.4	0.87

TABLE II. Spin-Hamiltonian matrices describing the E_1' center as determined from data obtained at 300 K. Measurement errors were less than 0.02 G for the experimental line positions and less than 0.5° for the angles at which data were taken. Since the matrices are all nearly axial, uncertainties are much larger in the angles specifying the nonunique principal directions.

Matrix	Principal values (from Silsbee[a])	Principal values (present study)	Principal directions (present study) θ	ϕ	Number of angles line positions	Root-mean-squares deviation (MHz)
$\overleftrightarrow{g}$	2.001 76	2.001 79	114.5°	227.7°	10,26	0.098
	2.000 49	2.000 53	134.5°	344.4°		
	2.000 29	2.000 30	125.4°	118.7°		
$\overleftrightarrow{A}_{strong}$	1271 MHz	−1269.72 MHz	114.1°	229.7°	10,52	0.163
	1091 MHz	−1095.02 MHz	128.3°	340.4°		
	1091 MHz	−1094.53 MHz	132.1°	115.9°		
$\overleftrightarrow{A}_{1,weak}$	27.43 MHz	−27.53 MHz	140.7°	284.5°	10,41	0.104
	22.00 MHz	−22.27 MHz	125.5°	133.9°		
	22.00 MHz	−22.14 MHz	104.6°	33.1°		
$\overleftrightarrow{A}_{2,weak}$	25.81 MHz	−26.01 MHz	58.9°	260.9°	10,43	0.097
	20.66 MHz	−21.04 MHz	104.4°	179.9°		
	20.66 MHz	−20.91 MHz	35.0°	111.4°		

[a]Reference 2.

Si(0) and Si(1) about the missing O(1) and to place an unpaired electron into the sp^3 hybrid orbital extending toward the vacancy from Si(0). They showed that Si(1) would relax away from the vacancy while Si(0) relaxed toward the vacancy and that the unpaired electron would be localized on only Si(0). Their model required only a single oxygen vacancy and has become generally accepted.

TABLE III. Atomic position coordinates at 298 K and the corresponding bond lengths and directions. (Obtained from Ref. 19.)

	X (Å)	Y (Å)	Z (Å)
Si(0)	2.3094	0.0	0.0
O(1)	1.3758	−1.1396	−0.6423
O(2)	1.3758	1.1396	0.6423
O(3)	3.2409	0.6217	−1.1598
O(4)	3.2409	−0.6217	1.1598
Si(1)	1.3031	−2.2571	−1.8021
Si(2)	1.3031	2.2571	1.8021
Si(3)	3.7610	2.0000	−1.8021
Si(4)	3.7610	−2.0000	1.8021
	Bond length (Å)	θ	ϕ
Si(0)→O(1)	1.6071	113.6°	230.7°
Si(0)→Si(1)		126.1°	246.0°
Si(1)→O(1)	1.6122	44.0°	86.3°
Si(1)→Si(0)		53.9°	66.0°
Si(2)→O(2)	1.6122	136.0°	273.7°
Si(2)→Si(0)		126.1°	294.0°
Si(3)→O(3)	1.6071	66.4°	249.3°
Si(3)→Si(0)		53.9°	234.0°
Si(4)→O(4)	1.6071	113.6°	110.7°
Si(4)→Si(0)		126.1°	126.0°

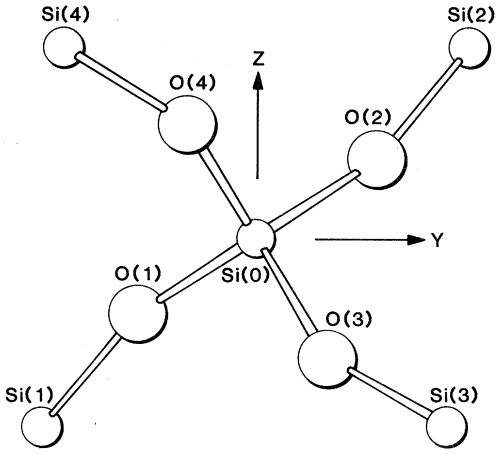

FIG. 8. Projection of the α-quartz lattice on the plane perpendicular to the X axis of the crystal. Labels for the various ions are used in the text to describe particular aspects of the E_1'-center models.

Although there is no doubt that an unpaired electron in an sp^3 hybrid orbital extending into a single vacancy is the primary component of the E_1' center, the two similar weak ^{29}Si hyperfine interactions do not appear to agree with this model. In the framework of the model just described it is difficult to find ^{29}Si nuclei which would have nearly identical magnitudes of hyperfine interactions. If the silicon nucleus directly across the vacancy from the unpaired electron gives rise to one of the weak hyperfine interactions, it is difficult to find only a single second silicon neighbor to give the remaining comparable weak interaction. On the other hand, the three silicons bonded to the Si(0) through the oxygen ions, O(2), O(3), and O(4), are all expected to be nearly equivalent. Thus, if they are responsible for the weak hyperfine interaction, there should be three such interactions instead of two.

One consistent way to interpret the weak hyperfine interactions is to assume a second missing oxygen. This leaves two nearly equivalent oxygen ions bonded to the primary silicon (i.e., the silicon on which the unpaired electron is localized) and thus allows a transferred hyperfine through the oxygens to two silicons via a superexchange interaction. In Fig. 8, this would correspond to O(1) and O(4) being missing, the unpaired electron being on Si(0) and extending into the vacancy O(1), and the two weak hyperfine interactions being with Si(2) and Si(3). Although not characterized in the present study, a very weak ^{29}Si hyperfine interaction has been observed[2] and could be attributed to Si(1) located across the primary vacancy from the unpaired electron. A comparison of the unique axis directions of the weak hyperfine matrices with the Si(2)→O(2) and Si(3)→O(3) bond directions shows reasonable agreement (see Table III). An estimate of the magnitude of the ^{29}Si hyperfine interaction arising through a superexchange effect can be obtained from the E_4' center, which is a similar oxygen-vacancy-type defect in quartz.[20]

In an early study of defects in quartz, Weeks[21] suggested a divacancy model for the E_1' center. However, at that time no supporting evidence was available for the presence of divacancy-type centers. In the recent study by Bossoli *et al.*[18] three similar but distinct oxygen-divacancy centers have been reported and their evidence suggests that oxygen divacancies are present in all as-grown synthetic quartz as a result of the growth process.

If a second oxygen vacancy is a part of the E_1' center, it should be considered as a perturbation to the primary oxygen vacancy and its associated unpaired electron. Difficulties arise when one speculates about the contents of the second vacancy (i.e., does it contain two electrons?) and, thus far, no firm evidence is available to resolve such questions. An important consideration is that the total charge of the defect must not deviate far from the lattice charge it replaces. Also, when considering the existence of the second vacancy and its contents, one must be aware of the relatively complex production and stabilization characteristics of the E_1' center that have been illustrated in this paper.

ACKNOWLEDGMENTS

This work was supported by the U.S. Air Force under Contract No. F19628-80-C-0086 with the Deputy for Electronic Technology (RADC), Hanscom Air Force Base, and monitored by Dr. Alton F. Armington.

[1]R. A. Weeks, J. Appl. Phys. 27, 1376 (1956).
[2]R. H. Silsbee, J. Appl. Phys. 32, 1459 (1961).
[3]F. J. Feigl, W. B. Fowler, and K. L. Yip, Solid State Commun. 14, 225 (1974).
[4]K. L. Yip and W. B. Fowler, Phys. Rev. B 11, 2327 (1975).
[5]R. A. Weeks and C. M. Nelson, J. Am. Ceram. Soc. 43, 399 (1960).
[6]J. G. Castle, D. W. Feldman, P. G. Klemens, and R. A. Weeks, Phys. Rev. 130, 577 (1963).
[7]F. J. Feigl and J. H. Anderson, J. Phys. Chem. Solids 31, 575 (1970).

[8]D. L. Griscom, E. J. Friebele, and G. H. Sigel, Jr., Solid State Commun. 15, 479 (1974).
[9]V. P. Solntsev, R. I. Mashkovtsev, and M. Ya. Schlerbakova, Zh. Strukt. Khim. 18, 729 (1977) [J. Struct. Chem. (USSR) 18, 578 (1977)].
[10]G. Gobsh, H. Haberlandt, H.-J. Wechner, and J. Reinhold, Phys. Status Solidi B 90, 309 (1978).
[11]A. V. Shendrik and D. M. Yudin, Phys. Status Solidi B 85, 343 (1978).
[12]D. L. Griscom, Phys. Rev. B 20, 1823 (1979).
[13]D. L. Griscom, Phys. Rev. B 22, 4192 (1980).
[14]J. D. H. Donnay and Y. Le Page, Acta Crystallogr. Sect. A 34, 584 (1978).
[15]M. E. Markes and L. E. Halliburton, J. Appl. Phys. 50, 8172 (1979).
[16]B. T. Smith, J. M. Boyle, J. J. Dongarra, B. S. Garbow, Y. Ikebe, V. C. Klema, and C. B. Moler, in *Matrix Eigensystem Routines-EISPACK Guide,* Vol. 6 of *Springer Lecture Notes in Computer Science,* 2nd ed., edited by G. Goos and J. Hartmanis (Springer, New York, 1976).
[17]S. P. Doherty, J. J. Martin, A. F. Armington, and R. N. Brown, J. Appl. Phys. 51, 4164 (1980).
[18]R. B. Bossoli, M. G. Jani, and L. E. Halliburton, Solid State Commun. 44, 213 (1982).
[19]Y. Le Page and G. Donnay, Acta Crystallogr. Sect. B 32, 2456 (1976).
[20]J. Isoya, J. A. Weil, and L. E. Halliburton, J. Chem. Phys. 74, 5436 (1981).
[21]R. A. Weeks, Phys. Rev. 130, 570 (1963).